

## CATALOG OF CANDIDATES FOR QUASARS AT $3 < z < 5.5$ SELECTED AMONG X-RAY SOURCES FROM THE 3XMM-DR4 SURVEY OF THE XMM-NEWTON OBSERVATORY

© 2018 г. G.A. Khorunzhev<sup>\*1</sup>, R.A. Burenin<sup>1</sup>, A.V. Mescheryakov<sup>1</sup> and S.Yu. Sazonov<sup>1</sup>

Preprint Accepted

We have compiled a catalog of 903 candidates for type 1 quasars at redshifts  $3 < z < 5.5$  selected among the X-ray sources of the serendipitous *XMM-Newton* survey presented in the *3XMM-DR4* catalog (the median X-ray flux is  $\approx 5 \times 10^{-15}$  erg s<sup>-1</sup> cm<sup>-2</sup> in the 0.5–2 keV energy band) and located at high Galactic latitudes  $|b| > 20^\circ$  in Sloan Digital Sky Survey (*SDSS*) fields with a total area of about 300 deg<sup>2</sup>. Photometric *SDSS* data as well infrared *2MASS* and *WISE* data were used to select the objects. We selected the point sources from the photometric *SDSS* catalog with a magnitude error  $\delta m_{z'} < 0.2$  and a color  $i' - z' < 0.6$  (to first eliminate the M-type stars). For the selected sources, we have calculated the dependences  $\chi^2(z)$  for various spectral templates from the library that we compiled for these purposes using the EAZY software. Based on these data, we have rejected the objects whose spectral energy distributions are better described by the templates of stars at  $z = 0$  and obtained a sample of quasars with photometric redshift estimates  $2.75 < z_{\text{phot}} < 5.5$ . The selection completeness of known quasars at  $z_{\text{spec}} > 3$  in the investigated fields is shown to be about 80%. The normalized median absolute deviation ( $\Delta z = |z_{\text{spec}} - z_{\text{phot}}|$ ) is  $\sigma_{\Delta z / (1 + z_{\text{spec}})} = 0.07$ , while the outlier fraction is  $\eta = 9\%$ , when  $\Delta z / (1 + z_{\text{spec}}) > 0.2$ . The number of objects per unit area in our sample exceeds the number of quasars in the spectroscopic *SDSS* sample at the same redshifts approximately by a factor of 1.5. The subsequent spectroscopic testing of the redshifts of our selected candidates for quasars at  $3 < z < 5.5$  will allow the purity of this sample to be estimated more accurately.

**DOI:** 10.1134/S1063773716050042

**Keywords:** quasars, X-ray surveys, photometric redshift

### INTRODUCTION

Searching for quasars at  $z \gtrsim 3$  is one of the most important elements of studying the growth history of supermassive black holes and the evolution of massive galaxies in the Universe. To improve the available constraints on the models of the X-ray luminosity function for quasars at  $z \gtrsim 3$  requires collecting a large X-ray sample of distant quasars at high redshifts (see, e.g., Aird et al., 2015). Bright and distant quasars are rare objects, with X-ray surveys of large area and sufficient depth being needed for their search. Photometric and spectroscopic support at optical wavelengths is required to work with X-ray sources. An increasing role of the methods for estimating the photometric redshift to determine  $z$  and to classify the sources is traceable in present-day works on this subject matter Assef et al. (2011); Civano et al. (2012); Kalfountzou et al. (2014).

In their recent paper, Kalfountzou et al. (2014) constructed the X-ray luminosity function for quasars at  $z > 3$  based on a catalog of 209 X-ray sources detected in various sky fields with a total area of  $\approx 33$  deg<sup>2</sup>. This catalog consists of two parts: *C-COSMOS* is a Chandra X-ray survey with an area of 0.9 deg<sup>2</sup>, 122 sources with fluxes  $2 \times 10^{-16} < F_X < 2 \times 10^{-15}$  erg s<sup>-1</sup> cm<sup>-2</sup> (Elvis et al., 2009) and *ChaMP* is a "serendipitous" survey based on CHANDRA pointings with area 33 deg<sup>2</sup>, 87 sources with fluxes  $3 \times 10^{-15} < F_X < 3 \times 10^{-14}$  erg s<sup>-1</sup> cm<sup>-2</sup> (Kim et al., 2007). The *C-COSMOS* survey has deep photometric (using a set of medium-band filters) and spectroscopic coverage and, for this reason,  $\approx 90\%$  identification completeness of objects at  $z > 3$ . The spectroscopic *ChaMP* program (44 objects) and various photometric relations (43 objects) were used to measure and estimate the

<sup>1</sup>Here and below, all X-ray fluxes and luminosities are given in the 0.5–2 keV energy band.

\*Электронный адрес: horge@iki.rssi.ru

redshifts of *ChAMP* sources. Thus, objects with firmly established redshifts may be deemed to constitute about 70% of the sample of quasars at  $z > 3$  from Kalfountzou et al. (2014).

The observations of numerous astrophysical objects with the *XMM-Newton* X-ray telescope accumulated for the last 15 years collectively represent a unique "serendipitous" X-ray sky survey (Watson et al., 2009) with a total area of about  $800 \text{ deg}^2$  and a sensitivity of  $\approx 5 \times 10^{-15} \text{ erg s}^{-1} \text{ cm}^{-2}$  (the *3XMM-DR4* version; Watson et al., 2009, 2013). It is hoped that a sample of quasars at  $z > 3$  selected by their X-ray emission that exceeds the sample of Kalfountzou et al. (2014) by several times will be obtained on the basis of this survey. This is the goal of our work.

Photometric and spectroscopic support is required to work with the X-ray sources from the *3XMM-DR4* catalog. The solution of the problem is facilitated by publicly accessible surveys: the optical photometric and spectroscopic Sloan Digital Sky Surveys (*SDSS*, Alam et al., 2015; Aihara et al., 2011; Eisenstein et al., 2011) with areas of  $\approx 14000$  and  $\approx 10000 \text{ deg}^2$ , respectively; the infrared photometric *2MASS* (Cutri et al., 2003) and *WISE* (Wright et al., 2010) all-sky surveys.

The spectra were taken and the redshifts were measured for a large number of distant quasars as part of the spectroscopic *SDSS* programs. Therefore, it is natural to use the spectroscopic sample of *SDSS* objects (Alam et al. 2015) as the first step:  $\approx 60000$  quasars with  $z_{\text{spec}} > 3$  on  $\approx 10000 \text{ deg}^2$ . However, the spectroscopic *SDSS* is based on a fairly complex method for the selection of quasar candidates whose completeness and purity depend on many factors: the redshift, the morphological properties of objects, the quality of photometry, etc. (Ross et al., 2013). The purity of the samples of distant quasar candidates for the *SDSS* does not exceed 50% (Ross et al., 2012). At the same time, it is unclear how the completeness and purity of the selection of candidates for the spectroscopic *SDSS* program behave as a function of the X-ray flux.

The technique of comparing the spectral energy distribution of a source in the optical and infrared bands with the template spectra of quasars, stars, and galaxies can be used for the selection of quasar candidates at  $z > 3$  among the X-ray sources of the *3XMM-DR4* survey. Such a technique not only gives the probability that the object is a quasar but also allows its photometric redshift estimate  $z_{\text{phot}}$  to be obtained. In the case of quasars at high redshifts,  $z > 3$ , the reliability of their

redshift estimates based on optical data increases, because the jump produced by the bright  $\text{Ly}\alpha$  line and the  $\text{Ly}\alpha$  forest in the quasar spectrum fall into the optical band. The addition of infrared *WISE* photometry increases the purity of the sample of distant quasar candidates and gives an advantage over the selection methods based only on *SDSS* photometry.

In this paper, we present the sample of candidates for quasars at  $z > 3$  obtained by searching for such objects among the X-ray sources of the serendipitous *XMM-Newton* survey, *3XMM-DR4*, using *SDSS*, *2MASS* and *WISE* data. The properties of this sample are discussed. Subsequently, we are going to use this sample to construct the X-ray luminosity function for quasars  $z > 3$ . Here, we use the following cosmological parameters:  $\Omega_0=0.3$ ,  $\Lambda_0=0.7$ ,  $H_0=70 \text{ km s}^{-1} \text{ Mpc}^{-2}$ .

#### THE SAMPLE OF X-RAY SOURCES WITH OPTICAL AND INFRARED PHOTOMETRY

In our work, we used data from the *3XMM-DR4*<sup>2</sup> (Watson et al., 2013). Our sample consists of 129541 point (*SC\_Extent=0*) X-ray sources at Galactic latitudes  $|b| > 20^\circ$  and has an area of  $\approx 300 \text{ deg}^2$ , which is determined by the area of the overlap between the *3XMM-DR4* survey and the *SDSS*; the area is calculated below. We work with the 0.5–2 keV X-ray flux (the sum of columns *SC\_EP2\_FLUX* and *SC\_EP3\_FLUX* in the *3XMM-DR4* catalog).

We cross-correlated the catalog of X-ray sources with the data from the photometric (data release 10) and spectroscopic (data release 12) *SDSS* (Aihara et al., 2011; Ahn et al., 2012; Alam et al., 2015; Eisenstein et al., 2011). Within the  $2\sigma$  X-ray source position error (if it was less than  $3''$ , then within  $3''$ ) we searched for all optical *SDSS* sources. As a result, we produced a catalog of 64714 X-ray sources that have an optical counterpart among the *SDSS* objects. At the same time, 2489 (4%) X-ray sources have more than one optical counterpart. In the case of an ambiguous correspondence, we estimated  $z_{\text{phot}}$  for all the possible optical counterparts of a given X-ray source. It turns out that there are spectroscopic data for 12823 ( $\approx 20\%$  of the sample) X-ray sources in the *SDSS*. We deemed the spectroscopic redshift measurement reliable at the flag *zWarning=0*. It turns out that 390 sources in the *3XMM-DR4*

<sup>2</sup><http://heasarc.gsfc.nasa.gov/W3Browse/xmm-newton/xmmssc.html>

catalog have  $z_{\text{spec}} > 3$  and  $z_{\text{Warning}}=0$ ; 280 of them have a magnitude measurement error  $\delta m_{z'} < 0.2$  (see below).

We additionally made a cross-correlation with the catalog of quasars from Flesch (2015). This catalog contains the spectroscopically confirmed X-ray quasars the data on which were published before January 25, 2015, and the sample of reliable (the probability that  $>99\%$  will turn out to be a quasar) photometric candidates from Bovy и др. (2012); Richards et al. (2009). We added 49 objects with  $z > 3$  from the catalog of Flesch (2015), five of them with photometric  $z$  estimates (Richards et al., 2009). As a result, we obtained a spectroscopic sample of 329 quasars with redshifts greater than 3 (280 from the spectroscopic SDSS sample and 49 from Flesch (2015)). This sample is required to check the completeness of our sample of quasars (see below).

We searched for infrared counterparts in the *2MASS* (Cutri et al., 2003) and *WISE* (Wright et al., 2010) catalogs. The search was made within 6 arcsec of the X-ray source position. If we found no infrared counterpart for an optical source, then we set  $7\sigma$  and  $5\sigma$  limits for the *2MASS* photometric  $J$ ,  $H$ ,  $Ks$  bands and *WISE* photometric  $w1$ ,  $w2$ ,  $w3$ ,  $w4$  bands, respectively, using the photometric data for adjacent sources. For the *2MASS* and *WISE* sources that were not detected in all bands, we used the upper limits from the corresponding catalogs. We assumed that the *2MASS* sources always corresponded to the sources with *WISE* photometry. When a *WISE* source was offset from an *SDSS* source by more than 2 arcsec, then we additionally considered the case where the source had only *SDSS* photometry when calculating  $z_{\text{phot}}$ . In this case, the upper limits in the *2MASS* and *WISE* filters were taken to be equal to the *WISE/2MASS* magnitudes of the controversial source.

Thus, we have a flux measurement or an upper limit on the flux in 12 broad bands ( $u'$ ,  $g'$ ,  $r'$ ,  $i'$ ,  $z'$ ,  $J$ ,  $H$ ,  $Ks$ ,  $w1$ ,  $w2$ ,  $w3$ ,  $w4$ ) for the X-ray sources. To calculate the fluxes in all photometric bands, we used the magnitudes designed to measure the fluxes from point sources, which the distant quasars are. In addition, the search was made only among the point *SDSS* sources.

There is no photometry for bright stars in the *SDSS*. To take into account their influence on our quasar selection method, we searched for the counterparts of *XMM*-Newton X-ray sources within 6 arcsec in the Guide Star Catalog (*GSC*, Lasker et al., 1990). This catalog was produced

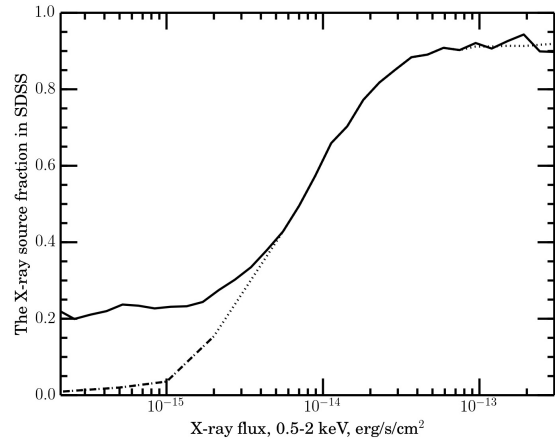


**Fig. 1.** The solid line indicates the fraction of X-ray sources in the *3XMM-DR4* catalog that were detected in the photometric *SDSS* ( $\delta m_{z'} < 0.2$ ) or that have a counterpart in the *GSC* as a function of the X-ray flux. The dashed line (at low X-ray fluxes) indicates the fraction of quasars at  $z > 3$  from *COSMOS* (Kalfountzou et al., 2014) detected in the photometric *SDSS*. The dots indicate the detection completeness function for X-ray quasars at  $z > 3$  in the *SDSS* composed from these two dependences and used below versus the X-ray flux.

by processing survey plates from the Palomar (northern hemisphere), Siding Spring (southern hemisphere), and several more observatories. The *GSC* contains  $\sim 19$  million sources with magnitudes from 6 to 16 (note that the sources brighter than magnitude 15 are overexposed in the *SDSS*), some of which were astrometrically classified as stars.

The fraction of X-ray sources in the *3XMM-DR4* catalog for which there are optical counterparts in the photometric *SDSS* and the *GSC* drops with decreasing X-ray flux from  $\approx 80\%$  at  $F_X \approx 10^{-14}$   $\text{ergs}^{-1} \text{cm}^{-2}$  to  $\approx 20\%$  at  $F_X \approx 10^{-15}$   $\text{ergs}^{-1} \text{cm}^{-2}$ . At lower X-ray fluxes, the fraction of nearby galaxies ( $z < 1$ ) in the sample of X-ray sources increases (Lehmer et al., 2012); therefore, no further reduction in the detection completeness of objects in the *SDSS* occurs.

The quasars at  $z > 3$  constitute a small fraction of all X-ray sources, and the fraction of objects with optical counterparts for them can differ from that for all X-ray sources. This assumption can be tested using the representative sample of quasars with reliably measured  $z > 3$  from the deep C-COSMOS X-ray survey that was talked about above. Out of 122 objects in this sample, 32 have spectroscopic redshifts  $z_{\text{spec}}$ , 75 have reliable

photometric redshifts  $z_{\text{phot}}$  (measured with a set of medium-band filters), and 15 have no optical counterpart to  $m_{i'} \approx 28$  and, therefore, are also deemed probable candidates for quasars at  $z > 3$  (Kalfountzou et al., 2014; Civano et al., 2011). Figure 1 shows how the fraction of objects from this sample detected in the photometric SDSS changes with X-ray flux. The fraction of objects with optical counterparts detected in the SDSS among the quasars at  $z > 3$  turns out to be lower than that for all X-ray sources at fluxes below  $2 \times 10^{-15} \text{ erg s}^{-1} \text{ cm}^{-2}$  by several times.

Below, when taking into account the influence of object detection incompleteness in the photometric SDSS on our final sample of candidates for quasars at  $z > 3$ , we use an approximate smooth photometric completeness function of the X-ray flux composed from the dependence for the detection completeness of quasars at  $z > 3$  at fluxes below  $2 \times 10^{-15} \text{ erg s}^{-1} \text{ cm}^{-2}$  and the corresponding dependence for all X-ray sources at fluxes above  $5 \times 10^{-15} \text{ erg s}^{-1} \text{ cm}^{-2}$  (see Fig. 1).

#### PHOTOMETRIC DATA FITTING BY SPECTRAL TEMPLATES

In our work, to calculate the  $\chi^2$  при values when fitting the spectral energy distribution in the optical and infrared bands by various spectral templates and to obtain the photometric redshift estimates, we used the *EAZY* (Brammer et al., 2008). This software steps through a grid of redshifts and at each  $z$  finds the best-fitting synthetic template by minimizing the  $\chi^2$  value:

$$\chi^2 = \sum_{j=1}^{N_{\text{filt}}} \frac{(T_{z,i,j} - F_j)^2}{(\delta F_j)^2}, \quad (1)$$

where  $N_{\text{filt}}$  is the number of photometric data points (filters),  $T_{z,i,j}$  is the synthetic flux of template  $i$  at redshift  $z$  in filter  $j$ ,  $F_j$  — is the observed flux in filter  $j$  and  $\delta F_j$  — is the flux error that takes into account the photometric error in filter  $j$ .

The *EAZY* software implements an algorithm that allows one to seek a superposition of several spectral templates, for example, the spectra of a galaxy and a quasar. However, we use only a one-template fit in our work, because we search for bright quasars whose emission dominates over the emission from the host galaxy. The quasars are characterized by a large scatter of spectra and strong variability (see e.g., Richards et al., 2006); therefore, it is necessary to have a sufficiently

complete template library.

For each object, we made separate iterations for the libraries of quasar and star templates. When fitting by the quasar templates, we corrected the SDSS photometry for extinction in our Galaxy using its values for each object from the photometric SDSS catalog. For the star templates, the SDSS photometry was not corrected for extinction in our Galaxy. The best value of  $z_{\text{phot}}$  was sought on the grid of redshifts  $[0.01, 7]$  with a 0.01 step by finding the best-fitting template from the library of quasars according to the  $\chi^2$  test.

We also took into account the intergalactic absorption by neutral hydrogen (Madau, 1995). The intergalactic absorption allows for the influence of the Ly $\alpha$  forest on the spectral energy distribution of a quasar. At redshifts  $z > 3$ , Ly $\alpha$  forest absorbs a substantial fraction of light on the blue side of the Ly $\alpha$  line, and this fraction increases with redshift. At such redshifts, the Ly $\alpha$  line falls into the photometric  $g'$  band, and the presence of a jump in the Ly $\alpha$ -forest absorption can already be determined from  $u' - g'$  color. At redshifts above  $z \approx 3.5$ , the Ly $\alpha$  line moves into the  $r'$  band, and the presence of an absorption jump is determined from the  $g' - r'$ . This feature in the spectra of quasars at redshifts  $z > 3$  allows one to increase the identification reliability of such objects and to obtain more reliable photometric estimates of their redshifts (see below).

#### The Template Library

The targets of our search are type 1 quasars (without any significant intrinsic absorption) at  $z > 3$ . We used the spectral templates of quasars from the *EAZY* (Brammer et al., 2008) and *LePHARE* (Ilbert et al., 2006) libraries as well as from other libraries (Assef et al., 2010; Richards et al., 2006; Krawczyk et al., 2013). The templates that we modified (Krawczyk et al., 2013) were added to the library. In these templates, we took into account the contribution of the quasar's emission lines obtained from the template (Vanden Berk et al., 2001). Besides, we extended the average spectrum of SDSS quasars (Vanden Berk et al., 2001) to the infrared ( $\lambda > 8000 \text{ \AA}$ ) using the template of a type 1 active galactic nucleus (AGN) (Assef et al., 2010) and added the resulting template to our library. We also added the templates of an elliptical galaxy (Assef et al., 2010) and a type 2 quasar (Polletta et al., 2007). As in (Dahlen et al., 2013), we applied the set of extinctions  $E(B - V) = 0.01, 0.05, 0.5$  and  $1.0$  according to the law of (Calzetti et al., 2000)

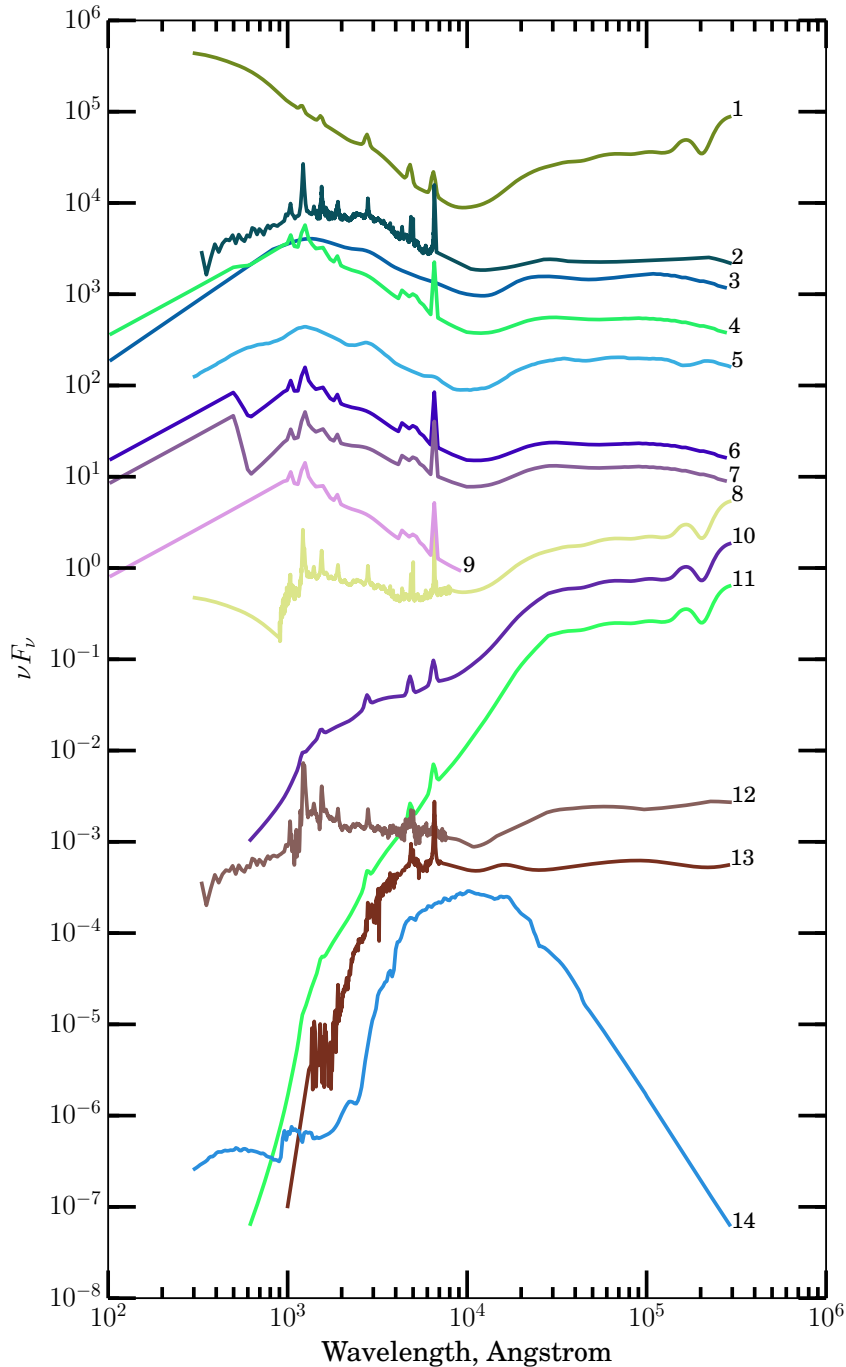


**Fig. 2.** Templates from the library of quasars in relative units  $\nu F_\nu$ : 1 – the average spectrum of type 1 quasars (Assef et al., 2010), 2 – the average spectrum of *SDSS* quasars (Brammer et al., 2008), 3 – the average spectrum of luminous type 1 quasars (Krawczyk et al., 2013), 4 – the average spectrum of type 1 quasars (Krawczyk et al., 2013) supplemented by emission lines with extinction  $E(B - V) = 0.01$ , 5 – the average spectrum of type 1 quasars (variant 2) (Assef et al., 2010), 6 – the average spectrum of type 1 quasars (Krawczyk et al., 2013), supplemented by emission lines with extinction  $E(B - V) = 0.05$ , 7 – the average spectrum of type 1 quasars (Krawczyk et al., 2013), supplemented by emission lines with extinction  $E(B - V) = 0.1$ , 8 – the template of a type 1 quasar extended to the infrared Vanden Berk et al. (2001), 9 – the average spectrum of type 1 quasars (Krawczyk et al., 2013) truncated to fit only the optical part, аппроксимации только оптической части, 10 – template 1 (Assef et al., 2010) with extinction  $E(B - V) = 0.5$ , 11 – template 1 (Assef et al., 2010) with extinction  $E(B - V) = 1.0$ , 12 – the composite quasar template from the spectra of the deep *VIMOS-VLT* survey (Gavignaud et al., 2006; Ilbert et al., 2006), 13 – the spectrum of an obscured type 2 quasar Polletta et al. (2007), 14 – the spectrum of an elliptical E0 galaxy (Assef et al., 2010).

using tabulated data from the *LePHARE* software package (Ilbert et al., 2006) to the templates.

We tested the template library on the spectroscopic *SDSS*-DR12 sample and eliminated those templates that more often erroneously classified a nearby object as an object at  $z > 3$  than correctly classified distant quasars from the template library. Thereafter, 14 templates remained, which were subsequently used to search for quasars at  $z > 3$ . These templates are presented in Fig. 2.

The galaxy and obscured quasar templates are needed only to eliminate the nearby objects whose accurate redshift is of no interest to us. In this case, no additional templates of galaxies (star-forming ones, with a different contribution of the active nucleus, etc.) are required to be applied, because this will increase the number of outliers and degrade the completeness and purity of the final sample of quasars at  $z > 3$  (Simm et al., 2015; Salvato et al., 2009).

For the templates of stars, we used the library of spectra from Pickles (1998). It includes the spectra of spectral types *O*, *A*, *B*, *F*, *G*, *K*, *M*. For some of the templates, there is a breakdown into luminosity classes: i – supergiants, ii – luminous giants, iii – giants, iv – subgiants, v – main-sequence stars. The library spectra were constructed only to a wavelength of  $2.5 \mu\text{m}$  Pickles (1998). Since the *WISE* filters are longer-wavelength ones, each spectrum from this library was extrapolated by Planck’s law for black-body radiation to a wavelength of  $30 \mu\text{m}$ . Such assumption works well for single main-sequence stars hotter than M0.

#### *Criteria for the Selection of Quasar Candidates* $3 < z < 5.5$

Since the quasars are star-like objects, we consider only the point *SDSS* sources when searching for distant quasars. In this case, the contamination of the sample by M-type stars presents a significant problem. Many of them are detected in the *XMM*-Newton X-ray survey owing to their coronal activity. During flares, the ratio of the X-ray and optical/near-IR fluxes for M dwarfs can be the same as that for quasars.

The *SDSS* sensitivity in the blue filters is insufficient to separate distant quasars with  $i' \gtrsim 20.5$  from stars. M dwarfs can be separated from distant quasars only by the  $i' - z'$  (Richards et al., 2002; Wu et al., 2012; Skrzypek et al., 2015): the stars have  $i' - z' > 0.8$ , while the quasars have  $i' - z' < 0.4$ . The color for the quasars  $i' - z' < 0.4$  remains approximately constant up to a redshift of  $\approx 5.5$ ,

until the  $\text{Ly}\alpha$  line passes from  $i'$  to  $z'$ . The color of the quasars then becomes  $i' - z' \approx 2$ . The quasars at  $z \gtrsim 5.5$  have reliable photometry only in one *SDSS* band, and, in that case, the method of determining  $z_{\text{phot}}$  by template fitting works poorly. Therefore, to increase the purity of our sample of quasar candidates, we used a constraint on the sensitivity in the  $z'$  *SDSS* band and the  $i' - z'$  color:

$$\delta m_{z'} < 0.2 \ \& \ i' - z' < 0.6, \quad (2)$$

where  $\delta m_{z'} < 0.2$  is the error in the apparent magnitude of a point source in the  $z'$  *SDSS* filter.

The constraint  $\delta m_{z'} < 0.2$  help to reduce the selection effects in searching for quasars. The spectral energy distribution of quasars rises from  $\lambda \approx 1 \mu\text{m}$  to  $\text{Ly}\alpha$ . The relations between the threshold sensitivities of the filters in the *SDSS* are such that by imposing the constraint (2), we guarantee the detection completeness of type 1 quasars not only in the  $z'$  filter but also in bluer *SDSS* filters.

After applying the photometric constraints, the quasar candidates are selected according to the condition:

$$\chi_{star}^2 / \chi_{qso}^2 > 1 \ \& \ z_{\text{phot}} > 2.75 \quad (3)$$

where  $\chi_{star}^2$  is the smallest  $\chi^2$  value for the template from the library of stars, and  $\chi_{qso}^2$  is the primary minimum of the  $\chi^2$  distribution for the quasar templates.

The conditions  $\chi_{star}^2 / \chi_{qso}^2 > 1$  and  $i' - z' < 0.6$  eliminate 97% of the stars among the X-ray sources of the *3XMM-DR4* catalog. This was tested on stars for which the *SDSS* spectra are available (see Fig. 3).

There exists a scatter of  $z_{\text{phot}}$  relative to  $z_{\text{spec}}$ . Hence, some of the objects with  $z_{\text{spec}} > 3$  will have  $z_{\text{phot}} \lesssim 3$ ; therefore, we chose the lower limit  $z_{\text{phot}} > 2.75$  when compiling the catalog of candidates for quasars at  $z > 3$ .

We additionally checked our sample of quasar candidates to eliminate, where possible, the source misidentification errors. We excluded 20 objects from the sample: two stars with the *SDSS* spectra, several faint sources against the background of a nearby bright galaxy, faint sources near a bright star, and objects with erroneously measured redshifts.

#### *Examples of Objects from the Catalog*

Figures 4 and 5 provide several examples of photometric data fitting by quasar and star

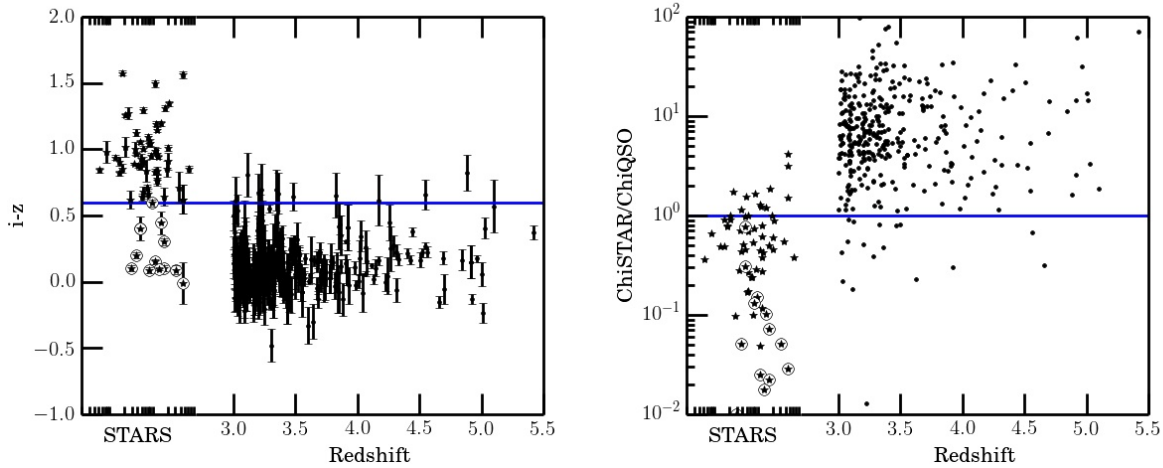


**Fig. 3.** Criteria for selection by the  $i' - z'$  *SDSS* (left) and  $\chi_{star}^2/\chi_{qso}^2 > 1$  (right) versus redshift. The solid horizontal lines indicate the boundaries of the selection criteria. The dots indicate 329 quasars with  $z_{spec} > 3$ . The symbol  $\star$  indicates 66 spectroscopically confirmed stars from *SDSS* DR12 that have a minimum of the  $\chi^2(z_{phot})$  distribution at  $z_{phot} > 3$ . The circles mark the stars with the same color  $i' - z' < 0.6$  as that for the quasars.

templates for known quasars (for which  $z_{spec}$  is available) or stars. Figures 4 and 5 present, respectively, the cases where one of the quasar spectral templates describes well the photometric data points and gives a nearly correct estimate of  $z_{phot}$  and where quasar template fitting leads to a misidentification and gives an unreliable estimate of  $z_{phot}$ . The corresponding  $\chi^2(z)$  distributions are shown in the insets.

The objects *3XMM J151147.1+071406* ( $z_{spec} = 3.481$ ), *3XMM J001115.2+144601* ( $z_{spec} = 4.964$ ), and *3XMM J004054.6-091527* ( $z_{spec} = 5.020$ ) are examples where the photometric redshift estimation method works well. In this case, the signal detection in infrared filters guarantees that the object is not a star.

The object *3XMM J153322.7+324351* is an example of a poor redshift determination:  $z_{phot} = 3.01$ . The true value measured in the *SDSS* is  $z_{spec} = 1.897$ .

The object *3XMM J080630.4+153241* is an M-type star. It was not included in our catalog of quasar candidates, because  $i' - z' > 0.6$  and  $\chi_{qso}^2/\chi_{star}^2 > 1$  for this object. If an object with a similar color relation is fainter by two apparent magnitudes, i.e., near the *SDSS* detection threshold, then the sensitivity of the *WISE* and *2MASS* surveys will be insufficient for its detection. In that case, the star and quasar templates will describe the *SDSS* photometric data points with comparable  $\chi^2$  values, and the star may be mistaken for a quasar at  $z_{phot} > 3$ . Nevertheless,

many of such objects can be eliminated using the photometric constraints (2).

The object *3XMM J094109.9+344902* lies at  $z_{spec} = 2.643$ . There is a *WISE* source more than 2 arcsec away from the *SDSS* source. Two photometric redshift estimates were made for this object: by taking into account the fluxes measured in *WISE* and *2MASS* filters and using these values only as upper limits on the infrared flux (see above). In the former case,  $z_{phot} = 2.62$  (template 12 was used in fitting) and the object does not enter into the catalog of quasar candidates, because  $z_{phot} < 2.75$ . In the latter case,  $z_{phot} = 3.00$  (template 1 was used) and, as a result, the object enters into the catalog. Such cases degrade the catalog purity.

## THE CATALOG AND ITS PROPERTIES

According to the selection rules described above, we compiled a catalog of 903 candidates for quasars at  $3 < z < 5.5$ . These include 21 *3XMM*-DR4 pointing targets. The catalog is presented in the Appendix in the form of a table where the coordinates, X-ray fluxes, photometric and spectroscopic (if available) redshifts, the best quasar and star templates are given. The properties of the catalog and its spectroscopic subsample are reflected in Fig. 6.

The objects in the catalog mostly have photometric redshifts  $2.75 \lesssim z_{phot} \lesssim 3.5$ . The objects have following distributions by  $z_{phot}$ : 381 at  $3 \lesssim z_{phot} \lesssim 4$ ; 60 at  $4 < z_{phot} \leq 5$ ; 2 at  $z_{phot} > 5$ .

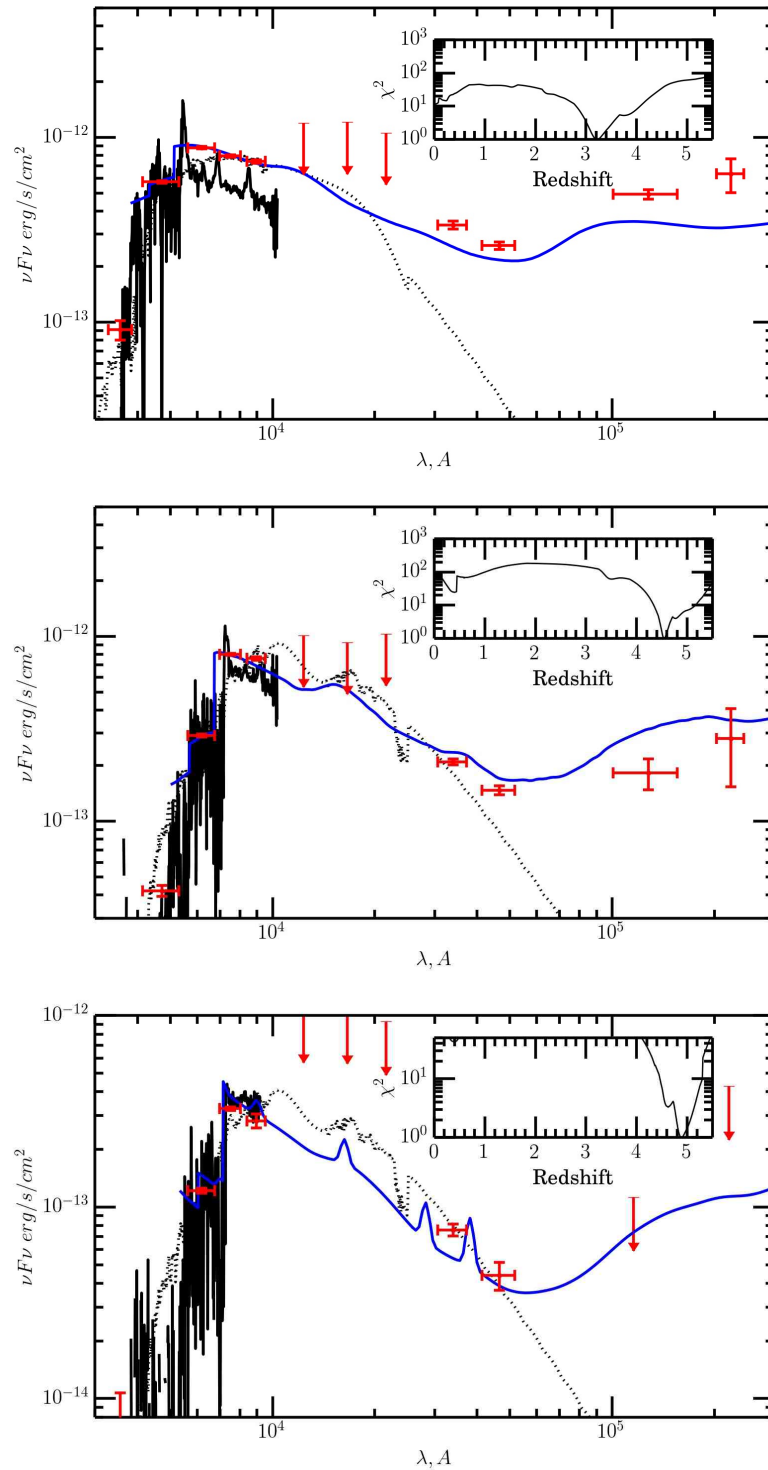


**Fig. 4.** Examples of a satisfactory determination of the photometric redshift. Top: *3XMM J151147.1+071406* is a quasar,  $z_{\text{spec}} = 3.481$ ,  $z_{\text{phot}} = 3.22$ . Middle: *3XMM J001115.2+144601* is a quasar,  $z_{\text{spec}} = 4.964$ ,  $z_{\text{phot}} = 4.54$ . Bottom: *3XMM J004054.6-091527* is a quasar,  $z_{\text{spec}} = 5.020$ ,  $z_{\text{phot}} = 4.88$ . The *SDSS* spectrum (black solid line), the photometric data points with their errors (red), the template of a quasar at  $z_{\text{phot}}$  (blue solid line), and the template of a star (black dots) are shown. The  $\chi^2(z)$  distribution when fitting the photometric data by quasar templates is shown in the insets.

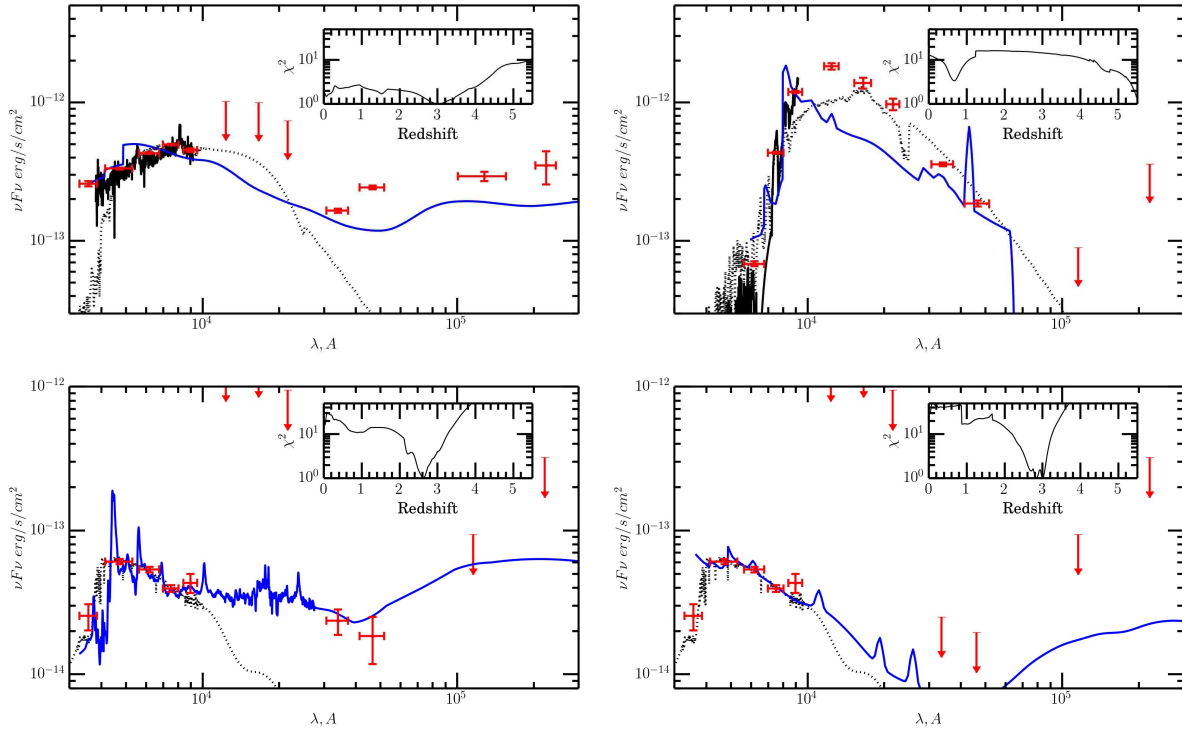


**Fig. 5.** Example of an unreliable estimation of the photometric redshift. Upper left: *3XMM J153322.7+324351* is a quasar at  $z_{\text{spec}} = 1.897$ . Its photometry is best described by the template of a type 1 quasar with  $z_{\text{phot}} = 3.06$ . Upper right: *3XMM J080630.4+153241* is an M-type star with  $z_{\text{phot}} = 5.58 \pm 0.02$ . The object was correctly classified as a star and was not included in the catalog of quasar candidates, because  $i' - z' > 0.6$  and  $\chi_{qso}^2 > \chi_{star}^2$  for it. Bottom left and right: *3XMM J094109.9+344902* is a quasar at  $z_{\text{spec}} = 2.643$ , for which two photometric redshift estimates were obtained due to its controversial association with a *WISE*:  $z_{\text{phot}} = 2.62$  and  $z_{\text{phot}} = 3.00$ ). The designations are the same as those in Fig. 4.

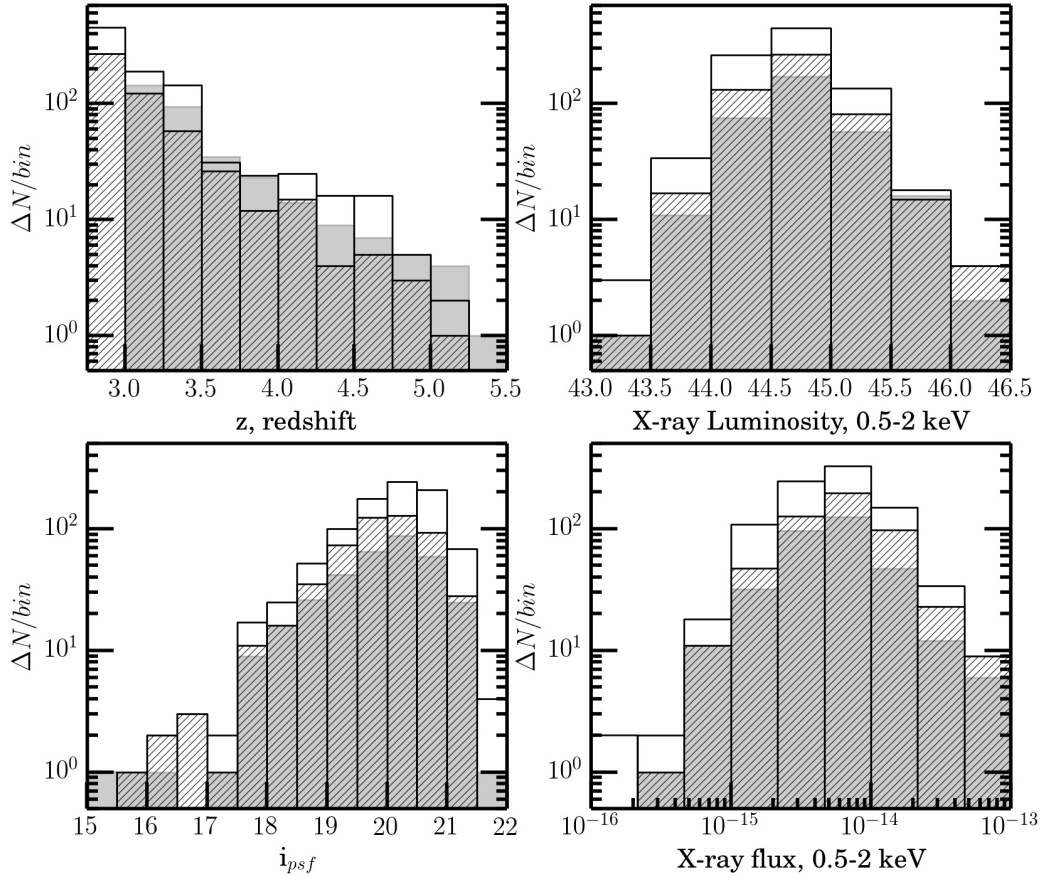


**Fig. 6.** Upper left: the distribution of quasar candidates in photometric redshift ( $z_{\text{phot}}$ ). Upper right: the distribution in the common logarithm of X-ray luminosity (in the 0.5–2 keV energy band in the observer’s frame), Lower left: the distribution in  $i'$  *SDSS* magnitude. Lower right: the distribution in X-ray 0.5–2 keV flux. The white color indicates the distributions for the entire catalog of quasar candidates. The hatching indicates the objects with  $z_{\text{phot}}$  that have known spectroscopic redshifts (with any  $z_{\text{spec}}$ ). The gray color indicates the known quasars with  $z_{\text{spec}} > 3$ . Their distributions were constructed from the spectroscopic redshifts ( $z_{\text{spec}}$ ). The height of each column is the total number of objects of the corresponding subsample in a given bin along the X axis.

The catalog contains 515 known quasars with reliably measured  $z_{\text{spec}}$ ; 266 of them have  $z_{\text{spec}} > 3$ . The photometry for these 515 objects is described by the template of a quasar at  $z_{\text{phot}} > 2.75$  and “passes” according to the selection criteria (see above). However, 63 known quasars with  $z_{\text{spec}} > 3$  (Flesch, 2015; Alam et al., 2015) did not satisfy the selection criteria. Their list is given in a separate table in the Appendix. Their photometric data points are most often better described (with smaller  $\chi^2$ ) by the star template or the template of a quasar at lower  $z$ . Some of the objects with  $z_{\text{spec}} > 3$  in the *SDSS* are classified as extended sources. No reliable spectroscopic redshift measurements are available

for 388 distant quasar candidates.

The median X-ray flux for the objects from the catalog (903 sources) is  $5.3 \times 10^{-15} \text{ erg s}^{-1} \text{ cm}^{-2}$  in the 0.5–2 keV energy band. All sources with fluxes above  $4 \times 10^{-14} \text{ erg s}^{-1} \text{ cm}^{-2}$  have spectroscopic redshifts. Because of the constraint on the error in the  $z'$  *SDSS* magnitude and the requirement  $i' - z' < 0.6$ , most of our objects turn out to be brighter than magnitude 21.5 in the  $i'$  *SDSS* filter.

Thus, our catalog of candidates for distant quasars can (as a result of the subsequent spectroscopic testing) lead to a noticeable (up to a factor of 1.5) increase in the number of known X-ray quasars at  $z > 3$  relative to the already existing

spectroscopic sample (in the same sky fields).

### THE PHOTOMETRIC REDSHIFT ACCURACY, THE CATALOG COMPLETENESS AND PURITY

The accuracy of the photometric  $z_{\text{phot}}$  estimates for distant quasar candidates can be investigated based on a sample of 329 quasars with known spectroscopic redshifts  $z_{\text{spec}} > 3$  (Fig. 7). It is convenient to estimate the scatter of  $z_{\text{phot}}$  relative to  $z_{\text{spec}}$  (see, e.g., Hoaglin и др. 1983, Salvato et al. 2009) via the normalized median absolute deviation of  $\Delta z = |z_{\text{phot}} - z_{\text{spec}}|$ :

$$\sigma_{\Delta z/(1+z_{\text{spec}})} = 1.48 \times Me\left(\frac{|z_{\text{phot}} - z_{\text{spec}}|}{(1 + z_{\text{spec}})}\right), \quad (4)$$

In our case (for quasars with known  $z_{\text{spec}} > 3$ ),  $\sigma_{\Delta z/(1+z_{\text{spec}})} = 0.07$ . In this case, the percentage of outliers, the fraction of objects with  $|z_{\text{phot}} - z_{\text{spec}}|/(1 + z_{\text{spec}}) > 0.2 \approx 3\sigma_{\Delta z/(1+z_{\text{spec}})}$  turns out to be  $\eta = 9\%$ .

Note that the standard confidence intervals for the EAZY photometric redshift were underestimated (Dahlen et al., 2013; Hildebrandt et al., 2008). Only for about of  $\approx 30\%$  the objects from our sample do the spectroscopic redshifts lie within the  $2\sigma$  error in  $z_{\text{phot}}$  (determined in a standard way from the change in  $\chi^2$  near its minimum). Therefore, we will use only  $\sigma_{\Delta z/(1+z_{\text{spec}})}$  in discussing the photometric redshift accuracy.

As regards the completeness of our catalog of distant quasar candidates, to a first approximation, it can also be estimated based on the spectroscopic sample of 329 known quasar at  $z_{\text{spec}} > 3$ . For this purpose, consider the ratio of the number of objects from this sample for which a good photometric redshift estimate was obtained,  $|z_{\text{phot}} - z_{\text{spec}}|/(1 + z_{\text{phot}}) < 0.2$ , to the total number of objects from the spectroscopic sample at a given  $z$ .

The catalog completeness estimated in this way is about 80% (the blue solid line in Fig. 8).

However, it is clear that this estimate cannot be deemed quite reliable, because the spectroscopic sample used was compiled only from optical data and can differ significantly in its properties from the X-ray quasar sample. Indeed, in our catalog, which was compiled on the basis of an X-ray survey, there are much more objects per unit sky area, some of which can be quasars at  $z > 3$ . Moreover, in estimating the completeness with respect to all X-ray quasars (at a given X-ray flux), we should

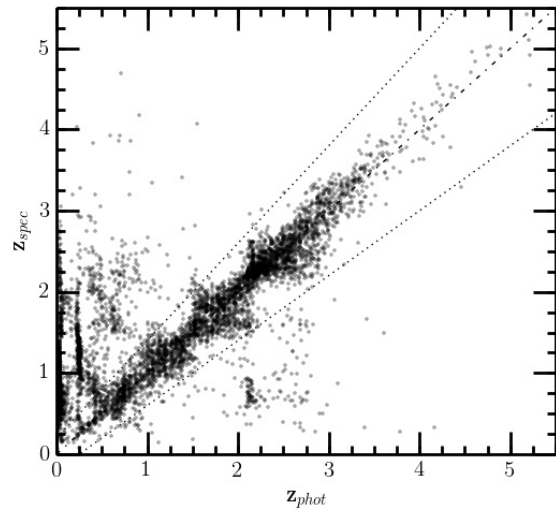


**Fig. 7.** Scatter of  $z_{\text{spec}}$  relative to  $z_{\text{phot}}$  for 6162 point objects from the spectroscopic *SDSS* catalog with  $z_{\text{spec}} < 5.5$  (having an error  $\delta z_{PSF} < 0.2$  in the *SDSS* filter). For 329 objects with  $z_{\text{spec}} > 3$  the scatter is  $\sigma_{\Delta z/(1+z_{\text{spec}})} = 0.07$ , the percentage of outliers is  $\eta = 9\%$  (see the determinations in the text). The dotted lines bound the region  $|z_{\text{phot}} - z_{\text{spec}}|/(1 + z_{\text{phot}}) < 0.2$ . The dash-dotted line indicates the straight line  $z_{\text{phot}} = z_{\text{spec}}$ .

also take into account the objects that are seen as X-ray sources in the 3XMM-DR4 survey but are too faint in the optical band and, therefore, enter neither into our catalog nor into the spectroscopic sample. To take into account all these possibilities requires performing the corresponding simulations of the quasar population, which we are going to do later on.

It will be possible to investigate the catalog purity, i.e., the ratio of the number of true quasars at  $z > 3$  to the number of all objects in the catalog, later on by performing spectroscopic observations of a representative subsample of objects from our catalog. By considering the ratio of the number of quasars from the spectroscopic sample that entered into our catalog to the number of all objects in the catalog, we can obtain a lower limit on the purity of our catalog, which is indicated in Fig. 8 by the red dashed line.

### THE X-RAY SURVEY AREA AND THE $\text{Log}N\text{-Log}S$ CURVE

The total geometric area of the overlap between the 3XMM-DR4 X-ray survey and the photometric *SDSS* is about  $\approx 300 \text{ deg}^2$  at Galactic latitudes  $|b| > 20^\circ$ . The survey area as a function of the X-ray flux can be estimated as the ratio of the total number

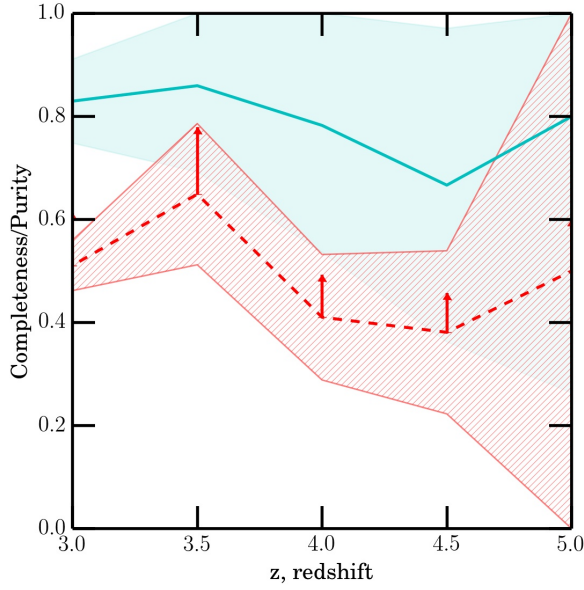


**Fig. 8.** Candidate selection completeness (the blue solid line and the corresponding  $1\sigma$  Poisson uncertainty region) and purity (the red dashed line and the corresponding uncertainty region) versus redshift in 0.5-wide bins. The plot was constructed relative to the spectroscopic sample (329 objects with  $3 < z < 5.5$ ). This dependence was constructed in 0.5-wide redshift bins. The arrows mean that the purity relative to the spectroscopic sample should be considered as a lower limit of the true purity, which is not yet known.

of *3XMM-DR4* X-ray sources in *SDSS* fields with an X-ray flux above a given one to the expected density of such sources in the sky. The expected density of sources at a given flux was calculated using the approximation from Mateos et al. (2008), where the statistics of *XMM-Newton* sources on a total area of  $132 \text{ deg}^2$  at high Galactic latitudes,  $|b| > 20^\circ$ , was analyzed in detail. The area estimate obtained in this way is presented in Fig. 9.

Using this estimate of the survey area as a function of the X-ray flux, we can construct the  $\log N$ – $\log S$  curve for quasar candidates at  $z > 3$ . To take into account the fact that not all quasars at  $z > 3$  among the *3XMM-DR4* X-ray sources are also seen in the optical *SDSS* images, the  $\log N$ – $\log S$  curve can be properly corrected. For this purpose, we can use the estimate of the fraction of X-ray quasars at  $z > 3$  having *SDSS* photometry at a given X-ray flux that was discussed above (see Fig. 1). The  $\log N$ – $\log S$  curve for quasars at  $z > 3$  was constructed as follows:

$$N(> S) = \sum_{i=1}^{N_S} \frac{1}{\Omega_i \alpha_i}, \quad (5)$$

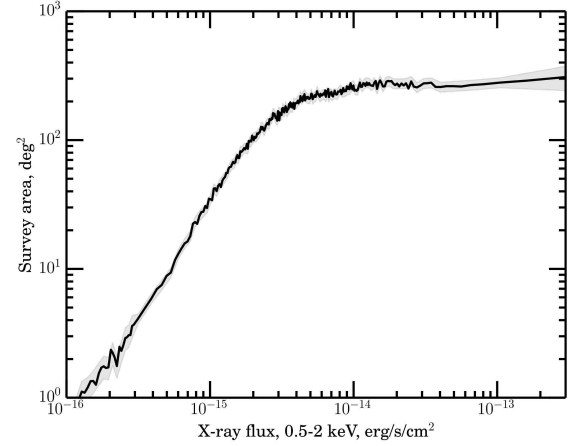


**Fig. 9.** Survey area (*3XMM-DR4*) versus X-ray flux (0.5–2 keV) in regions with *SDSS* coverage at Galactic latitudes  $|b| > 20^\circ$ . The gray region indicates the  $2\sigma$  Poisson errors.

with the corresponding error being

$$\sigma_N = \sqrt{\sum_{i=1}^{N_S} \left[ \frac{1}{\Omega_i^2 \alpha_i^2} + \left( \frac{\delta \alpha_i}{\Omega_i \alpha_i^2} \right)^2 \right]}, \quad (6)$$

where  $\Omega_i \equiv \Omega(S_i)$  is the survey area at flux  $S_i$ ,  $\alpha_i \equiv \alpha(S_i)$  is the fraction of X-ray quasars at  $z > 3$ , that have *SDSS* photometry, and the summation is over  $N_S$ -sources with fluxes  $S_i \geq S$ .

The  $\log N$ – $\log S$  curve constructed from all objects in our catalog is indicated in Fig. 10 by the black solid line. However, this curve actually does not reflect the true distribution of quasars at  $z > 3$  in X-ray flux, because quite a few objects with redshifts entered into our catalog and 63 quasars with  $z_{\text{spec}} > 3$  were missed. Therefore, Fig. 10 shows two more  $\log N$ – $\log S$  curves: only for the sources with  $z_{\text{spec}} > 3$  (dotted lines) and for the sources that do not have either the spectrum or  $z_{\text{spec}} > 3$  (dashed line). The true  $\log N$ – $\log S$  curve must lie between these two curves.

## CONCLUSIONS

We searched for quasar candidates at  $z > 3$  in the *3XMM-DR4* catalog of X-ray sources using a photometry of *SDSS*, *2MASS*, *WISE*. A catalog of 903 candidates for quasars with photometric redshifts  $z_{\text{phot}} > 2.75$  was compiled.

Note that several catalogs of candidates for quasars with photometric redshift estimates have already been produced previously based on data from the photometric *SDSS* catalog (see, e.g., Bovy и др. (2012); Richards et al. (2009)), and

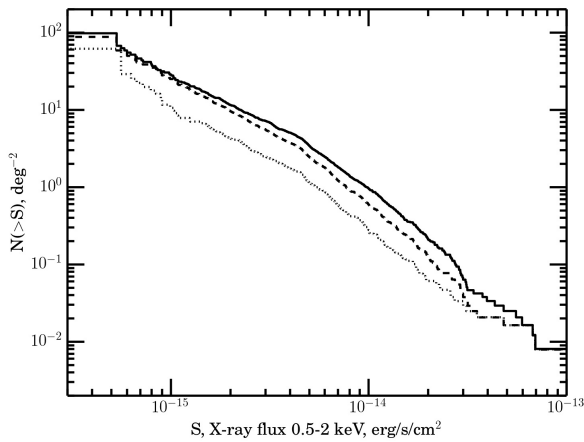


**Fig. 10.** The black solid line indicates the  $\text{Log}N\text{-Log}S$  distribution of candidates for quasars at  $z > 3$ . (i.e., with  $z_{\text{phot}} > 2.75$ ). The dotted and dashed lines indicate, respectively, the  $\text{Log}N\text{-Log}S$  distribution only for the objects from this sample with known spectroscopic redshifts  $z_{\text{spec}} > 3$  and for the objects with  $z_{\text{spec}} > 3$  or without  $z_{\text{spec}}$ . The true  $\text{Log}N\text{-Log}S$  curve for quasars at  $z > 3$  must lie between these two curves.

WISE data have also been used in their recent paper by DiPompeo (2015). Our quasar selection method differs fundamentally in that the selection results (the density of quasars in the sky) can be presented in the form of a dependence on the X-ray flux, which is important for the subsequent construction of the X-ray luminosity function. A preliminary comparison showed that our sample of candidates for quasars at  $z \sim 3$  is essentially identical (in the sky fields we investigated) to the sample from DiPompeo (2015). However, there are significant discrepancies between the samples at  $z \gtrsim 4$  whose degree and cause are to be investigated in a subsequent work.

Preliminary estimates of the selection quality using the *SDSS* DR12 catalog of spectroscopic redshifts (supplemented by quasars from the catalog published recently by Flesch (2015)) для рентгеновских источников *XMM*-Newton X-ray sources (*3XMM-DR4*) showed that the completeness of our sample is about 80% and its purity is at least 50%. However, these estimates are not quite reliable and must be checked in future through simulations of the quasar population and using optical observations of objects from this sample.

The accuracy of the photometric redshift estimates is  $\sigma_{\Delta z/(1+z_{\text{spec}})} = 0.07$  with  $\approx 9\%$  of outliers. This accuracy is comparable to other similar measurements based on photometric

*SDSS* data (see, e.g., Kitsionas et al., 2005). Such an accuracy is sufficient to measure the luminosity function. We are going to perform these measurements in our next work.

About half of the bright objects in our sample have measured redshifts. The objects in our sample have apparent magnitudes  $i' \lesssim 21.5$ . We began the spectroscopic observations of the remaining objects from this sample with the 6-m telescope at the Special Astrophysical Observatory of the Russian Academy of Sciences and with the 1.6-m telescope at the Sayan Observatory of the Institute of Solar– Terrestrial Physics, the Siberian Branch of the Russian Academy of Sciences, where a new medium- and low-resolution spectrograph well suited for such observations was installed (Burenin et al., 2016) These observations not only will allow the sample quality to be estimated but also will probably allow a large number of quasars at  $z > 3$  to be confirmed, which, in turn, will make it possible to measure more accurately the X-ray luminosity function for quasars.

It will be possible to apply the high-redshift quasar selection algorithms tested in our paper to select such objects among the X-ray sources of the SRG all-sky survey. As can be seen, in particular, from the results of our paper, it will be possible to detect of the order of several tens of thousands of quasars at  $3 < z < 6$  in the SRG survey. This unique observational material will allow the growth history of supermassive black holes at the epoch of active galaxy formation to be studied in detail.

#### ACKNOWLEDGMENTS

This study was supported by the Russian Science Foundation (project no. 14-22-00271). We would like to thank V. Astakhov for translation of the paper in English. The electronic version of the article’s tables is available <sup>3</sup> at the Vizier catalogue access tool, CDS, Strasbourg, France (Ochsenbein et al., 2000).

<sup>3</sup><http://adsabs.harvard.edu/abs/2016yCat..90420313K>

## СПИСОК ЛИТЕРАТУРЫ

1. C. Ahn, R. Alexandroff, P. Allende, S. Anderson, T. Anderton, B. Andrews, et al., *Astrophys. J. Suppl. Ser.* **203**, 21 (2012).
2. H. Aihara, C. Allende Prieto, D. An, S. F. Anderson, E. Aubourg, E. Balbinot, et al., *Astrophys. J. Suppl. Ser.* **193**, 29 (2011).
3. Aird et al. (J. Aird, A. Coil, A. Georgakakis, K. Nandra, G. Barro, P. Perez-Gonzalez), *MNRAS.* **451**, 1892 (2015).
4. S. Alam, F. Albareti, C. Prieto, F. Anders, S. Anderson, B. Andrews, et al., *Astrophys. J. Suppl. Ser.* **219**, 12 (2015).
5. R.J. Assef, C.S. Kochanek, M. Brodwin, R. Cool, W. Forman, A. Gonzalez, et al., *Astrophys. J.* **713**, 970 (2010).
6. R.J. Assef, C.S. Kochanek, M. Ashby, M. Brodwin, M. Brown, R. Cool, et al., *Astrophys. J.* **728**, 56 (2011).
7. D. Van den Berk, G. Richards, A. Bauer, M. Strauss, D. Schneider et al., *Astron. J.* **122**, 549 (2001).
8. J. Bovy, A. Myers, J. Hennawi, D. Hogg, R. McMahon, D. Schiminovich, et al., *Astrophys. J.* **749**, 41 (2012).
9. G. Brammer, P. van Dokkum, P. Coppi, *Astrophys. J.* **686**, 1503 (2008).
10. R. Burenin, A. Amvrosov, M. Eiselevich, V. Grigor'ev et al., *Astron. Letters* **42**, 295 (2016).
11. D. Calzetti, L. Armus, R. Bohlin, A. Kinney, J. Koornneef, T. Storchi-Bergmann, *Astrophys. J.* **533**, 682 (2000).
12. F. Civano, M. Elvis, M. Brusa, A. Comastri, M. Salvato, G. Zamorani, et al., *Astrophys. J. Suppl. Ser.* **201**, 30 (2012).
13. F. Civano, M. Brusa, A. Comastri, M. Elvis, M. Salvato, G. Zamorani, et al., *Astrophys. J.* **741**, 91 (2011).
14. R. Cutri, M. Skrutskie, S. van Dyk, C. Beichman, J. Carpenter, T. Chester, et al., The IRSA 2MASS All-Sky Point Source Catalog, NASA/IPAC Infrared Science Archive. **06**, <http://adsabs.harvard.edu/abs/2003tmc...book.....C> (2003).
15. T. Dahlen, B. Mobasher, S. Faber, H. Ferguson, G. Barro, S. Finkelstein, et al., *Astrophys. J.* **775**, 93 (2013).
16. M.A. DiPompeo, J. Bovy, A. Myers, D. Lang, *MNRAS.* **452**, 312 (2015).
17. D. J. Eisenstein, D. Weinberg, E. Agol, H. Aihara, C. Allende Prieto, S. F. Anderson, et al., *Astron. J.* **142**, 72 (2011).
18. M. Elvis, F. Civano, C. Vignali, S. Puccetti, F. Fiore, N. Cappelluti, et al., *Astrophys. J. Suppl. Ser.* **184**, 158 (2009).
19. E. W. Flesch, *Publications of the Astronomical Society of Australia* **32**, 010 (2015).; arXiv:1502.06303
20. I. Gavignaud, A. Bongiorno, S. Paltani, G. Mathe, G. Zamorani, P. Moller, et al., *Astron. Astrophys.* **457**, 79 (2006).
21. H. Hildebrandt, C. Wolf, N. Benitez, *Astron. Astrophys.* **480**, 703 (2008).
22. D.C. Hoaglin, F. Mosteller, J. W. Tukey, *Understanding Robust and Exploratory Data Analysis* (Wiley Series in Probability and Mathematical Statistics), New York, 1983.
23. O. Ilbert, S. Arnouts, H. McCracken, M. Bolzonella, E. Bertin, E. Bertin, et al., *Astron. Astrophys.* **457**, 841 (2006).
24. E. Kalfountzou, F. Civano, M. Elvis, M. Trichas, P. Green, *MNRAS.* **445**, 1430 (2014).
25. M. Kim, B. Wilkes, D. Kim, P. Green, W. Barkhouse, M. Lee, et al., *Astrophys. J. Suppl. Ser.* **169**, 401 (2007).
26. S. Kitsionas, E. Hatziminaoglou, A. Georgakakis, I. Georgantopoulos, *Astron. Astrophys.* **434**, 475 (2005).
27. C. Krawczyk, G. Richards, S. Mehta, M. Vogeley, S. Gallagher, K. Leghly, et al., *Astrophys. J. Suppl. Ser.* **206**, 4 (2013).
28. B. Lasker, C. Sruch, B. McLean, J. Russel, H. Jenkner, M. Shara, *Astron. J.* **99**, 2019 (1990).
29. B. Lehmer, Y. Xue, W. Brandt, D. Alexander, F. Bauer, M. Brusa, et al., *Astrophys. J.* **752**, 46 (2012).
30. S. Mateos, R. Warwick, F. Carrera, G. Stewart, J. Ebrero, R. Della, et al., *Astron. Astrophys.* **492**, 51 (2008).
31. A. Meshcheryakov, V. Glazkova, S. Gerasimov, R. Burenin et al., *Astron. Letters* **41**, 307 (2015).
32. P. Madau, *Astrophys. J.* **441**, 18 (1995).
33. F. Ochsenbein, P. Bauer, J. Marcout, *Astron. Astrophys. Suppl. Ser.* **143**, 23 (2000).
34. A. Pickles, *PASP* **110**, 863 (1998).
35. M. Polletta, M. Tajar, L. Maraschi, G. Trinchieri, C. Lonsdale, L. Chiappetti, et al., *Astrophys. J.* **663**, 81 (2007).
36. E. Wright, P. Eisenhardt, A. Mainzer, M. Ressler, R. Cutri, T. Jarrett, et al., *Astron. J.* **140**, 1868 (2010).
37. G. Richards, X. Fan, H. Newberg, M. Strauss, D. Vanden Berk, D. Schneider, et al., *Astron. J.* **123**, 2945 (2002).
38. G. Richards, M. Lacy, L. Storrie-Lombardi, P. B. Hall, S. Gallagher, D. Hines, X. Fan, *Astrophys. J. Suppl. Ser.* **166**, 470 (2006).
39. G. Richards, A. Myers, A. Gray, R. Riegel, R. Nichol, R. Brunner, et al., *Astrophys. J. Suppl. Ser.* **180**, 67 (2009).
40. N. Ross, A. Myers, E. Sheldon, C. Yeche, M. Strauss, B. Jo, et al., *Astrophys. J. Suppl. Ser.* **199**, 3 (2012).
41. N. Ross, I. McGreer, M. White, G. Richards, A. Myers, N. Palanque-Delabrouille, et al., *Astrophys. J.* **773**, 14 (2013).

42. M. Salvato, G. Hasinger, O. Ilbert, G. Zamorani, M. Brusa, N. Scoville, et al., *Astrophys. J.* **690**, 1250 (2009).
43. T. Simm, R. Saglia, M. Salvato, R. Bender, W. Burgett, K. Chambers et al., *Astron. Astrophys.* **584**, A106 (2015).
44. N. Skrzypek, S. Warran, J. Faherty, D. Mortlock, A. Burgasser, P. Hewett, *Astron. Astrophys.* **574**, 78 (2015).
45. D. Vanden Berk, G. Richards, A. Bauer, M. Strauss, D. Schneider, T. Heckman, *Astron. J.* **122**, 549 (2001).
46. M. Watson, A. Schroder, D. Fyfe, C. Page, G. Lamer, S. Mateos, et al., *Astron. Astrophys.* **493**, 339 (2009).
47. M. Watson et al., 3XMM-DR4 , (2013).
48. X. Wu, G. Hao, Z. Jia, Y. Zhang, N. Peng, *Astron. J.* **144**, 49 (2012).

## APPENDIX

*Catalog of candidates for quasars at  $3 < z < 5.5$ . The table of redshifts.*

N	NAME 3XMM	SRCID	RA	DEC	$F_{0.5-2}^{-14}$	$\Delta F_{0.5-2}^{-14}$	$i'_{PSF}$	$z'_{PSF}$	$z_{spec}$	$z_{ref}$	$z_{phot}$	FL	$T_Q$	$T_S$	NB
(1)	(2)	(3)	(4)	(5)	(6)	(7)	(8)	(9)	(10)	(11)	(12)	(13)	(14)	(15)	(16)
1	J000335.5-061112	119255	0.8981	-6.1869	2.851	0.205	19.25	19.00	2.8569	0(0)	3.05		4	f8i	7
2	J000303.7+020416	119783	0.7655	2.0714	1.295	0.211	20.76	20.33	2.9469	0(0)	3.02		12	g0iii	8
3	J000444.2+020801	117610	1.1846	2.1337	0.573	0.229	20.95	20.69	2.6655	0(0)	2.80		1	a7v	5
4	J000531.3+000840	117756	1.3806	0.1445	0.963	0.281	20.99	20.58	2.8480	0(0)	2.80		7	f5iii	7
5	J000443.6-084036	117599	1.1820	-8.6767	0.944	0.323	20.30	20.12			3.85		3	k3i	5
6	J000511.6-084201	117868	1.2986	-8.7005	0.498	0.185	19.64	19.64	3.2059	0(0)	3.30		1	f2v	7
7	J000533.7-084825	117722	1.3908	-8.8071	0.577	0.232	19.24	19.46			2.82		7	f8iv	8
8	J000618.1-084410	117240	1.5757	-8.7362	0.872	0.433	20.45	20.57	3.3234	0(0)	3.15		7	g0i	7
9	J000942.5+125251	118363	2.4272	12.8811	3.149	0.528	20.21	20.03	2.3926	0(0)	2.82		3	g8v	7
10	J001033.5+105231	118456	2.6398	10.8755	1.171	0.416	20.91	20.48	2.9202	0(0)	2.93		3	rk0v	7
11	J001037.5+105526	118489	2.6565	10.9239	1.463	0.406	20.25	20.04	2.6765	0(0)	2.81		1	f2v	5
12	J001115.2+144601	117909	2.8135	14.7671	10.810	0.299	18.28	18.10	4.9643	0(0)	4.54	t	5	m2i	9
13	J001340.4+054554	121657	3.4183	5.7651	0.927	0.213	19.95	19.85	2.7123	0(0)	2.97		1	f2iii	7
14	J001504.7+171517	121325	3.7700	17.2549	0.160	0.069	20.63	20.70	3.1627	0(0)	2.84		7	f6v	5
15	J001756.7+163007	122306	4.4864	16.5021	0.183	0.070	20.29	20.29	3.5487	0(0)	3.83		1	k3iii	6
16	J001920.9+163209	122068	4.8372	16.5359	0.859	0.167	19.04	19.00			2.96		1	f6v	8
17	J001754.1+161406	122310	4.4755	16.2350	0.465	0.136	20.81	20.45			2.87		3	wg5iii	8
18	J002015.9+214914	121995	5.0664	21.8208	0.346	0.120	19.72	19.51			3.03		12	k3iii	9
19	J002159.9-083503	120127	5.4996	-8.5843	0.236	0.092	20.78	20.72			2.84		12	rf6v	9
20	J002127.3-020333	120370	5.3640	-2.0593	1.829	0.154	17.00	16.90	2.596	1(824)	2.77	t	1	wf5v	12
21	J002150.6-150427	119878	5.4611	-15.0742	0.189	0.047	21.31	20.72			2.79		7	f5iii	5
22	J002208.0-150540	120066	5.5334	-15.0945	1.635	0.103	18.80	18.58	4.52	1(401)	4.40	t	4	m2i	7
23	J002244.4+013250	121123	5.6854	1.5474	0.915	0.105	19.51	19.38	2.9823	0(0)	2.76		2	f8iv	7
24	J002527.5+105118	120782	6.3648	10.8553	0.337	0.157	19.63	19.33			3.13		3	rk0iii	8
25	J002630.2+165656	113930	6.6259	16.9490	1.510	0.196	20.23	19.97	2.8593	0(0)	2.86		4	f5i	7
26	J002726.4+170730	113471	6.8602	17.1251	0.377	0.091	20.05	20.17	3.8857	0(0)	4.02		1	k2i	5
27	J002706.9+261559	113871	6.7791	26.2666	0.943	0.376	20.32	19.82			3.29		12	rk4iii	8
28	J003027.7+261355	19579	7.6157	26.2324	0.239	0.044	19.78	19.93	3.2136	0(0)	3.11		7	g0i	8
29	J003057.9+261744	16416	7.7415	26.2956	0.900	0.076	20.45	20.02			3.01		3	wg5iii	7
887	J233329.9+152539	237875	353.3750	15.4276	0.426	0.155	19.00	18.84	3.6508	0(0)	3.56		5	rk3iii	8
888	J233633.9+210442	238644	354.1413	21.0784	0.220	0.063	21.05	20.50			2.98		3	g8v	8
889	J233641.2+211955	238680	354.1717	21.3322	0.365	0.095	20.17	20.14			2.92		3	g8v	8
890	J234214.1+303606	237645	355.5590	30.6017	0.799	0.203	19.92	19.79			3.20	wD	2	wk2iii	5
891	J234309.6+001325	237594	355.7901	0.2239	0.470	0.110	20.59	20.83	2.8240	0(0)	2.96		9	f5i	5
892	J234448.7-042651	241540	356.2031	-4.4475	0.197	0.132	18.59	18.44			2.88	D	3	rg5iii	9
893	J234455.3+092444	241510	356.2304	9.4125	0.163	0.143	20.79	20.85			3.18	D	12	rg5iii	7
894	J234752.5+010306	242170	356.9688	1.0518	0.446	0.164	20.62	20.46	2.4114	0(0)	2.86		12	g0v	8
895	J234916.0+020722	241813	357.3167	2.1230	0.732	0.208	20.87	20.59	2.6551	0(0)	2.77		4	f0iii	5
896	J234956.8+363237	239836	357.4871	36.5437	0.548	0.203	19.55	19.40			2.92		3	wg8iii	8
897	J235054.6+200939	239972	357.7276	20.1609	1.000	0.121	18.49	18.47	3.1629	0(0)	2.88		6	f8i	12
898	J235201.3+200901	239304	358.0055	20.1506	1.163	0.151	18.37	18.33	3.0794	0(0)	3.09		1	g0iii	11
899	J235101.0+203504	240044	357.7544	20.5847	0.530	0.137	19.99	19.95			2.80		5	g0iv	8
900	J235111.2+202016	239889	357.7970	20.3378	0.996	0.358	20.11	19.86	2.329	0(0)	2.76		1	f02iv	7
901	J235435.5-101513	239560	358.6481	-10.2537	1.159	0.232	19.30	19.19	3.1203	0(0)	2.97		1	f5v	7
902	J235502.9+060825	240542	358.7623	6.1405	1.497	0.408	19.04	18.80	2.7077	0(0)	2.79		7	f8i	8
903	J235555.9+055933	240529	358.9831	5.9926	0.344	0.121	20.22	20.14			3.35		2	wk2iii	8

NAME is the name in the 3XMM-DR4 (3XMMJ...), SRCID is the unique X-ray source number in the 3XMM-DR4, RA is the right ascension and DEC is the declination in degrees in the 3XMM-DR4,  $F_{0.5-2}^{-14}$  and  $\Delta F_{0.5-2}^{-14}$  are the 0.5–2 keV flux and its error ( $\times 10^{-14}$  erg/s/cm<sup>2</sup>),  $i'_{PSF}$  is the apparent magnitude in the  $i'$  SDSS (AB, PSF),  $z'_{PSF}$  is the apparent magnitude in the  $z'$  SDSS filter (AB, PSF),  $z_{spec}$  is the spectroscopic redshift,  $z_{ref}$  is the number of the reference to the paper with published  $z_{spec}$  (0 – SDSS DR12, the zWarning flag is given in parentheses; 1 – the catalog of X-ray sources by Flesch (2015) the number of the data source from Flesch (2015) is given in parentheses),  $z_{phot}$  is the photometric redshift, FL is the data flag (D – there is another optical source within the  $2\sigma$  position error of the XMM X-ray source; w – the  $z_{phot}$  estimates were obtained only from the SDSS photometry, although there is a WISE source nearby; t – the XMM pointing target XMM, r – the star template describes the photometry better than does the quasar template ( $\chi^2_{Star}/\chi^2_{QSO} < 1$ ),  $T_Q$  is the template number from the quasar library,  $T_S$  is the star template (Pickles 1998) with the smallest  $\chi^2$ , NB – число фотометрических полос, используемых при аппроксимации. NB is the number of photometric bands used in fitting.

*Known quasars with  $z_{\text{spec}} > 3$  from the 3XMM-DR4 catalog that did not enter into our catalog of candidates*

N (1)	NAME 3XMM (2)	SRCID (3)	RA (4)	DEC (5)	$F_{0.5-2}^{-14}$ (6)	$\Delta F_{0.5-2}^{-14}$ (7)	$i'_{PSF}$ (8)	$z'_{PSF}$ (9)	$z_{\text{spec}}$ (10)	$z_{\text{ref}}$ (11)	$z_{\text{phot}}$ (12)	FL (13)	T <sub>Q</sub> (14)	T <sub>S</sub> (15)	NB (16)
1	J001049.0+290139	118405	2.7046	29.0277	0.275	0.192	20.23	20.18	3.370	0(0)	3.18	r	5	g2i	5
2	J002654.9+171944	113822	6.7289	17.3289	1.125	0.132	21.21	20.79	3.095	0(0)	2.72	r	12	f8i	7
3	J005156.6+272847	128940	12.9862	27.4799	0.289	0.183	19.73	19.57	3.331	0(0)	3.46	r	1	g5iv	7
4	J011117.7+325832	44045	17.8243	32.9758	0.245	0.099	19.59	19.39	3.205	1(1411)	0.69	r	13	m5iii	9
5	J011544.8+001513	125421	18.9371	0.2538	0.194	0.064	21.53	20.96	5.1	1(1245)	0.61	r	14	m4v	7
6	J020231.1-042246	43456	30.6301	-4.3794	1.285	0.279	20.68	20.43	4.270	0(0)	0.94	G	14	m7iii	9
7	J020253.7-065043	92295	30.7240	-6.8453	0.155	0.083	20.69	20.34	3.866	0(0)	0.79	G	13	m5iii	8
8	J020702.2-065233	96071	31.7593	-6.8759	0.366	0.111	20.51	20.45	3.065	0(0)	2.66	r	6	f0ii	7
9	J021338.6-051615	20962	33.4110	-5.2712	0.929	0.096	20.88	20.22	4.544	0(0)	0.55	r	14	m4iii	7
10	J021343.2-042042	107259	33.4301	-4.3450	0.347	0.163	20.45	20.38	3.074	0(0)	0.06	r	7	m5iii	7
11	J021504.1-040704	107902	33.7671	-4.1178	0.636	0.208	20.53	20.34	3.283	0(0)	0.03	r	6	f8i	7
12	J022048.5-033711	110418	35.2025	-3.6197	0.564	0.180	21.42	20.61	3.116	0(0)	2.71	r	12	f8i	7
13	J022251.7-050713	103134	35.7157	-5.1203	0.880	0.122	20.01	19.57	3.86	1(1758)	0.67	r	13	m3iii	8
14	J022645.4-043616	102470	36.6893	-4.6046	0.726	0.152	18.45	17.89	3.295	1(559)	0.49	r	14	m3iii	12
15	J022706.4-041924	105904	36.7769	-4.3235	0.392	0.100	20.65	20.60	3.285	1(650)	2.90	r	3	rg0v	5
16	J022849.6-043946	106357	37.2069	-4.6630	0.241	0.187	21.04	20.60	3.211	0(0)	2.62	r	7	f5i	7
17	J023226.0-053729	160738	38.1086	-5.6248	0.532	0.258	18.83	18.60	4.564	0(0)	0.28	r	14	m2iii	8
18	J024923.6-040206	163652	42.3484	-4.0351	0.391	0.195	20.81	20.62	3.029	0(0)	2.94	r	3	g5v	5
19	J030222.0+000630	155293	45.5921	0.1085	0.708	0.072	20.65	20.50	3.306	0(0)	0.03	r	13	k0iii	8
20	J030435.4-000250	156232	46.1476	-0.0474	0.605	0.241	20.41	20.16	3.055	0(0)	0.03	r	13	f8i	8
21	J080334.9+391923	79784	120.8954	39.3232	0.348	0.151	20.37	20.29	3.011	0(0)	2.67	r	7	f5i	7
22	J085026.7+630020	307591	132.6113	63.0057	0.647	0.195	18.36	18.23	3.363	0(0)	3.08	r	1	k3iii	11
23	J085809.3+274228	300636	134.5391	27.7080	0.246	0.052	20.39	20.48	3.464	0(0)	3.10	r	3	g8iv	5
24	J093521.2+612339	317819	143.8387	61.3943	0.693	0.101	20.04	20.12	4.042	0(0)	0.30	r	14	m2iii	7
25	J094013.9+344628	321396	145.0579	34.7747	2.295	0.257	21.35	20.90	3.355	0(0)	0.38	r	13	rk4iii	7
26	J094404.1+165056	322206	146.0174	16.8489	0.516	0.147	20.27	20.28	3.017	0(0)	3.05	r	1	f5iii	5
27	J095752.0+015119	313069	149.4669	1.8555	0.254	0.107	21.02	20.40	4.174	1(1886)	0.90	DG	14	m7iii	7
28	J100055.3+250907	310877	150.2306	25.1521	0.124	0.040	21.17	20.49	3.2	1(1538)	0.41	G	13	m3iii	8
29	J100226.1+024611	23727	150.6090	2.7687	0.428	0.057	20.06	20.19	3.038	1(271)	3.13	Gr	6	g2iv	5
30	J100655.8+050325	315437	151.7327	5.0571	1.454	0.644	19.46	19.39	3.086	0(0)	3.60	r	1	rk0v	8
31	J104445.6-011756	283334	161.1901	-1.2990	0.248	0.071	20.35	20.29	3.496	0(0)	3.73	r	1	g5i	5
32	J104920.9+510041	16951	162.3372	51.0114	0.171	0.034	20.87	20.77	3.057	0(0)	0.04	r	7	f5i	7
33	J104808.3+583718	275930	162.0347	58.6217	1.136	0.348	20.31	20.13	3.285	0(0)	0.05	r	13	wk2iii	8
34	J111151.3+061321	44028	167.9642	6.2227	0.146	0.031	20.18	20.33	3.200	0(0)	3.13	r	6	g0iv	5
35	J115659.3+551309	27772	179.2477	55.2190	0.933	0.234	18.39	18.09	3.110	0(0)	0.23	r	13	m1iii	12
36	J120613.4+443527	355201	181.5561	44.5908	0.564	0.114	20.93	20.28	3.483	0(0)	0.80	r	13	m5v	9
37	J120735.5+251140	356435	181.8982	25.1947	0.538	0.165	20.21	20.14	3.008	0(0)	2.73	r	7	f5i	7
38	J122652.2+013632	349269	186.7178	1.6090	0.687	0.201	19.61	19.74	3.015	0(0)	2.70	r	6	f02iv	8
39	J123142.1+110308	23419	187.9259	11.0522	0.382	0.045	20.06	20.00	3.024	0(0)	2.60	r	5	f02iv	7
40	J123231.0+121846	348272	188.1293	12.3131	0.302	0.153	20.57	20.69	3.055	0(0)	2.75	r	7	f5iv	7
41	J123613.4+275151	350816	189.0561	27.8643	0.424	0.106	20.10	20.07	3.780	0(0)	0.70	r	13	m3ii	11
42	J123752.6+092934	350323	189.4692	9.4930	0.925	0.216	19.60	19.54	3.027	0(0)	2.67	r	7	f02iv	7
43	J124405.1+125757	368647	191.0214	12.9659	1.101	0.200	21.15	20.86	3.1	1(611)	0.43	D	13	m2iii	7
44	J124825.2+673135	366095	192.1052	67.5266	0.519	0.101	19.15	19.10	3.224	0(0)	2.73	r	9	f8i	5
45	J130200.0+281213	362403	195.5002	28.2038	0.163	0.080	20.74	20.45	3.084	0(0)	2.68	r	2	f5iii	8
46	J130206.5+281117	362291	195.5272	28.1882	0.249	0.098	21.16	20.34	4.884	0(0)	5.55	r	12	m5v	8
47	J131047.8+322518	364785	197.6995	32.4219	0.090	0.048	20.34	19.96	3.009	0(0)	0.70	r	8	f0i	9
48	J132451.8+032722	331382	201.2159	3.4563	0.641	0.172	20.81	20.19	3.019	0(0)	3.22	r	12	wk2iii	7
49	J133002.2+241634	53129	202.5096	24.2766	0.192	0.055	20.75	20.21	3.038	0(0)	2.73	r	12	f2ii	7
50	J135613.7+182358	328590	209.0575	18.3996	0.482	0.087	21.10	20.68	3.927	0(0)	0.68	G	13	m3ii	8
51	J140149.8+024835	11017	210.4580	2.8100	0.982	0.073	21.19	20.53	3.83	1(643)	0.26	G	7	m2iii	7
52	J142437.8+225601	346440	216.1579	22.9338	41.066	10.834	15.39	15.34	3.62	1(1417)	3.57	G	7	rk3iii	12
53	J143023.7+420436	15580	217.5989	42.0768	54.979	0.640	19.16	19.31	4.656	0(0)	4.15	tr	1	m4v	5
54	J150603.5+012757	41624	226.5147	1.4664	0.787	0.136	20.78	20.36	3.852	0(0)	3.41	G	12	m2iii	7
55	J161618.1+122351	199481	244.0757	12.3976	0.223	0.137	20.00	19.73	4.292	0(0)	4.07	r	1	k3i	5
56	J164829.7+350159	29462	252.1238	35.0330	3.526	0.203	20.32	20.16	4.075	1(1347)	1.56	D	2	rf8v	7
57	J171456.2+593700	215090	258.7343	59.6168	1.198	0.398	20.52	20.17	4.028	1(1406)	0.24	r	6	g2v	8
58	J213621.4+003028	266573	324.0893	0.5079	0.602	0.082	20.54	20.09	3.2	1(1538)	0.18	G	12	wk2iii	7
59	J213729.8+003151	264414	324.3742	0.5310	0.263	0.043	20.97	20.80	3.630	0(0)	3.48	r	2	k01ii	5
60	J220814.9+015856	231039	332.0624	1.9824	0.713	0.375	19.71	19.52	3.084	0(0)	2.75	D	7	f5i	8
61	J220845.5+020252	235145	332.1896	2.0479	1.004	0.339	19.34	19.37	3.405	1(646)	1.38	3	wf5v	8	
62	J221722.2+001640	47709	334.3429	0.2780	0.088	0.019	21.28	20.61	3.366	0(0)	3.18	r	2	g2i	5
63	J224041.7+032326	223971	340.1738	3.3906	0.262	0.091	21.15	20.45	3.348	1(1880)	3.26	r	12	k3iii	6

The structure of the table and the notation are the same as those for the table above.